Optical Materials 38 (2014) 265–271

Contents lists available at ScienceDirect

Optical Materials

journal homepage: www.elsevier.com/locate/optmat

Fabrication and characterization of large-core Yb/Al-codoped fused silica waveguides using dry etching

Gil Atar [a,b,*], Orna Ternyak [c], Doron Greental [d], David Eger [a], Galina Chechelnitsky [d], Noa Mazurski [d], Shifra Gouta [a], Yehoudit Elbaz [a], Ariel Bruner [a], Bruno Sfez [a], Shlomo Ruschin [b]

[a] Applied Physics Division, Soreq NRC, Yavne 81800, Israel
[b] Department of Electrical Engineering—Physical Electronics, Faculty of Engineering, Tel Aviv University, Ramat Aviv, Tel Aviv 69978, Israel
[c] Micro- and Nano-Fabrication Unit (MNFU), Department of Electrical Engineering, Technion—Israel Institute of Technology, Haifa 32000, Israel
[d] The Center for Nano Science and Nanotechnology, Faculty of Science, The Hebrew University of Jerusalem, Jerusalem 91904, Israel

ARTICLE INFO

Article history:
Received 22 July 2014
Received in revised form 7 October 2014
Accepted 22 October 2014
Available online 14 November 2014

Keywords:
Fused silica
Dry etching
Al doping
Waveguide
Rare-earth doped silica

ABSTRACT

A deep inductively coupled plasma etching process was developed as a part of a continuous effort to develop an all-silica on-chip platform for high-power optical devices. Combined F and Cl based etching chemistry was found most suitable since silica matrix and Al doping are generally etched using different chemistries. First large-core (~20 × 20 μm) Yb/Al-codoped fused silica waveguides on pure silica substrate were successfully fabricated, featuring ~1 dB/cm optical propagation loss.

© 2014 Elsevier B.V. All rights reserved.

1. Introduction

The interest in the field of high-power lasers and its applications has rapidly grown in recent years. One of the main research efforts in the field is the development of optical devices to generate and manipulate high power light, for example laser sources [1], beam combiners [2], pulse compressors [3] and more. Some high-power optical devices are produced today using fiber technology or free-space optics, these methods presenting challenges in positioning, alignment and production. In contrast, on-chip devices fabricated employing lithography techniques offer high-level spatial accuracy, relatively fast transition from design to prototype, and standard production methods. For example, GaAs [4], Silicon-on-insulator [5], ion-exchanged glass [6] and silica-on-Silicon [7] are commonly used as platforms for various waveguide-based low-power optical devices in the field of telecommunication. However, developing a robust platform to make waveguide-based optical devices capable of carrying W-kW power levels has been a constant challenge.

The work reported here is part of a continuous effort to develop a platform for active/passive high-power optical devices based on Yb/Al-codoped fused silica (FS) waveguides (WG) on pure FS substrate. Yb doping (0.25 at.%) is required in order to fabricate active optical devices based on stimulated emission (amplifier/laser). Al doping (5–14 at.%) is introduced in order to facilitate Yb solubility in the silica matrix [8] and slightly raise the refractive index of the core to obtain light guiding.

In general, fabrication of waveguides is often made in two steps: fabrication of a bulk or layer structure, constituting a slab waveguide (1D light confinement) and patterning of the layer to create 2D waveguide structures forming an optical circuit. Successful fabrication of Yb/Al-codoped fused silica (FS) slab waveguide with high optical transmittance (0.2 dB/cm) and optical gain (0.6 dB/cm) was recently reported by our group [9]. A unique fabrication scheme was developed to meet the requirements for high-power waveguides such as high material damage-threshold, large core in order to minimize power-density, and good control over doping level to tailor the refractive index difference. In this report we account for the successful patterning of doped FS layer to create 2D WGs as well as the first large-core (20 × 20 μm) Yb/Al-codoped fused silica waveguide designed for high-power applications.

Various technologies are commonly used to create 2D waveguides from 1D layer structures [6,10], however most of them

* Corresponding author at: Applied Physics Division, Soreq NRC, Yavne 81800, Israel.
E-mail address: gilatar@soreq.gov.il (G. Atar).

http://dx.doi.org/10.1016/j.optmat.2014.10.048
0925-3467/© 2014 Elsevier B.V. All rights reserved.

are not suited for high-power devices since they typically produce relatively thin waveguides or are likely to lower material damage threshold [11]. In contrast, photolithography followed by plasma etching induces no physical or chemical changes in the core's bulk material, thus it is reasonable to assume that its intrinsic high damage-threshold remains unchanged. Deep etching capability is also highly attractive for making active devices such as laser sources since it allows complete removal of doped material outside the core area and use of non-doped clad material to avoid residual pump absorption. Another important advantage of photolithography-etching technique is a relatively rapid transition from optical design to device fabrication with $\lambda/100$ accuracy using standard fabrication methods. These inherent advantages provide strong motivation to develop novel plasma etching processes for high-power WG fabrication.

There are many reports on the use of reactive ion etching (RIE) and inductively coupled plasma etching (ICP) for the fabrication of low-power devices in thin layers of silica [12,13], however 20 μm deep ICP etching of Al-doped FS, as required for high-power optical devices in silica-on-silica (SOS) technology, presents a unique set of combined technological challenges: (a) mask material and patterning, (b) heat removal and (c) plasma composition. Conventional photoresist materials cannot serve as a mask for such deep and consequently long dry etching processes since it is not sufficiently resistive to plasma etching, therefore an exceptionally thick hard-mask is required. Heat buildup during long plasma etching processes is especially challenging in the case of FS substrates due to its low heat conductivity. Finally, the most challenging aspect in developing an ICP process for doped FS etching is the plasma composition and its compatibility to Yb/Al-codoped FS etching since silicon and aluminum oxides are generally etched using different gases. The existing processes are incompatible in the sense that each process used for one of the oxides is not effective or even induce damages to the other. At present we were not able to find any studies on plasma etching of compound silica-alumina glasses.

In this work successful 20 μm deep etching of Yb/Al-codoped FS was achieved using ICP, and the first large-core doped silica WG, suitable for high-power applications, was fabricated and characterized.

In the following report, our study of the physical and chemical aspects of Al doped silica plasma etching is presented. A fabrication scheme for making thick doped silica layers is reviewed in Section 2, with emphasis on material and physical considerations for high-power applications. Section 3 focuses on process development for deep etching of Yb/Al-codoped FS using ICP, offering a detailed analysis and material considerations. Preliminary optical WG transmittance measurements, showing 1–2 dB/cm propagation loss at 1030 nm for WGs with air cladding, are discussed in Section 4. The work reported here should constitute a significant step in developing a robust on-chip platform for high-power optical devices using SOS technology.

2. Fabrication of 1D doped silica layers

Fabrication of on-chip FS WG is based on fiber production methods, thus the first two steps are variations of the preform fabrication process (see Fig. 1): deposition of FS particles followed by amorphous sintering. Pure FS (Corning UV-grade 7980, $12 \times 12 \times 6.35\ mm^3$) is used as a substrate, on which a 100 μm thick layer of doped silica nanoparticles (soot) is formed by direct-nanoparticle-deposition (a version of the traditional flame hydrolysis) [14]. The soot contains Yb doping to achieve desired absorption level and a relatively high Al doping level to achieve full solubility of Yb doping and large index of refraction difference

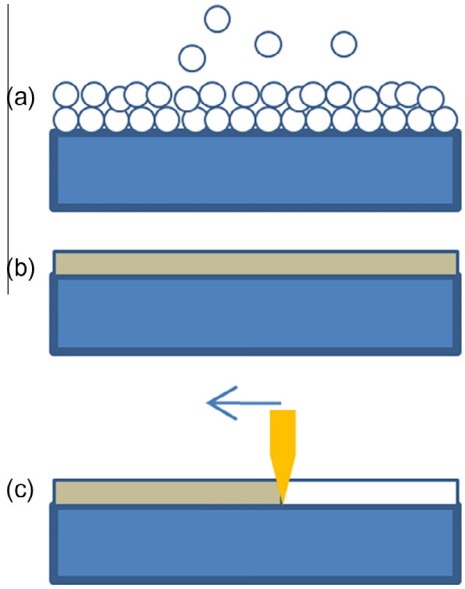

Fig. 1. Process flow for fabrication of Yb/Al-codoped fused silica layers on pure fused silica substrate. (a) Direct-nanoparticle deposition of doped silica particles on pure silica substrate, soot layer is 100 μm thick. (b) Amorphous sintering of soot to a ~20 μm thick silica layer containing structural defects and relatively high optical loss of 8 dB/cm. (c) Heat treatment ($T > 2000$ °C) by CO_2 laser scan. As a result, structural defects are eliminated and optical loss is reduced to 0.2 dB/cm.

(Δn). Density of deposited soot is about 5 times lower than that of FS. In the process of sintering, the sample is heated to 1500–1600 °C, where the soot layer undergoes amorphous densification to reach a final thickness of 20 μm. At this stage, the Yb/Al-codoped FS layer shows spectral characteristics of FS as reported in literature in terms of upper level lifetime and absorption cross section [15]. However, structural defects such as micron-scale voids, crystallites and surface roughness due to imperfect sintering induce large optical losses. A unique CO_2 laser heat treatment was developed to mitigate all three kinds of structural defects [16]. The fast absorption of FS at 10.6 μm rapidly heats the doped layer ($T > 2000$ °C) inducing diffusion of voids, amorphization of crystallites and significantly reduces surface roughness via surface-tension-driven melt-flow. As a result, optical quality is dramatically improved from 8 dB/cm to 0.2 dB/cm total loss.

3. Fabrication of 2D rectangular waveguides

3.1. Requirements

The basic requirement of the dry etching process is to successfully etch Yb/Al-codoped FS up to 20 μm depth with relatively smooth walls. The etch depth is required to make a large core while completely removing all doped silica from the clad area. The smoothness of the wall is required to avoid high propagation loss due to light scattering.

The main process challenge lies in the formulation of the gas mixture, since the silica matrix and Al doping (in the phase of Al_2O_3) are generally etched using different chemistries. In addition, the deep etching of FS requires use of hard masking material with sufficient etching selectivity. Thermal management issues should be seriously considered in the high density plasma etching of thermally isolating FS.

Fig. 2 shows the process flow for patterning rectangular doped FS WGs which is further detailed below. In essence, 2.5–3 μm Cr layer is sputtered on doped silica layer to serve as a hard mask. Positive photoresist is used for photolithography followed by wet

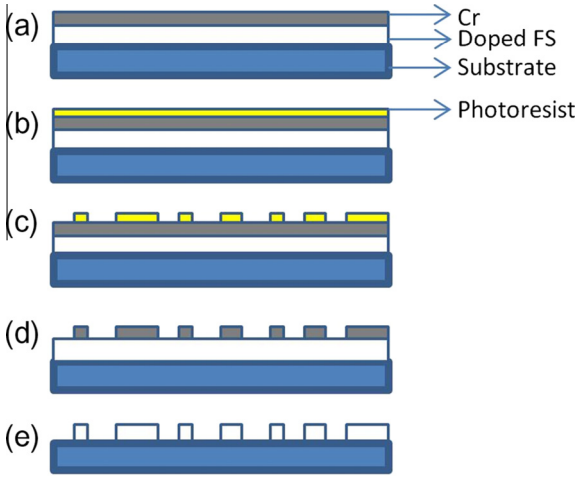

Fig. 2. Process flow for patterning doped FS WGs on pure FS substrate. (a) Cr layer sputtering (2.5 μm thick) on doped FS layer. (b) Photoresist spin coating (AZ1512 HS, 1.2 μm thick). (c) Photolithography followed by wet etching. (d) Wet etching of uncovered Cr domains using Cr etchant. (e) ICP etching of doped FS layer to create 20 μm thick doped FS WGs with varying widths (10–50 μm).

etching to remove only domains that were not exposed to light. Similarly, Cr etchant is used to remove Cr domains which are not covered by photoresist followed by a 2nd wet etch to remove photoresist residues and obtain required Cr mask. Finally, ICP etching is used to pattern 20 μm deep WG's.

3.2. Etching mask fabrication

The mask plays a dominant role in the resultant resolution, homogeneity and side-wall roughness. Mask material is chosen for its selectivity to etching chemistry, and mask thickness according to required etching depth. In the case reported here, a hard mask of 2.5 m thick Cr layer was found suitable. Line-edge roughness (LER) of the mask should be kept as low as possible since it will usually be transferred to the etched pattern. LER could be reduced by using a high-quality photolithography mask and optimizing the photolithography process parameters such as the type of photoresist, UV power and/or exposure time, and wet development conditions. Nevertheless, in the case of wet etching of polycrystalline metal (such as the case described here), the initial grain size of the metal layer might serve as the lower boundary for the mask's LER.

Sputtering was used to coat the Yb/Al-codoped FS layers with 2.5–3 μm thick polycrystalline Chromium. Coating was made using 1.8A and 350 V, for 45 min at 3 μTorr while allowing sufficient time for cooling every 10 min to avoid excessive heating. Positive photoresist (AZ1512 HS, 1.2 μm thick) was used for photolithography followed by wet Cr etching in standard commercial etchant. Fig. 3 shows the resultant Cr lines on doped FS layer.

3.3. Thermal management

The FS samples are being significantly heated during long plasma etching. Cooling during ICP takes place via convection, as a gas (in this case He) is forced to flow through a nozzle in the metal electrode (which is kept at room temperature by an external heat exchanger), impacting on the central-bottom of the carrier wafer. The etched sample is placed on the carrier wafer, which makes cooling process more difficult due to vacuum gap between the carrier and the sample. In early experiments (following the procedure outlined in line 1* of Table 1) FS substrates were

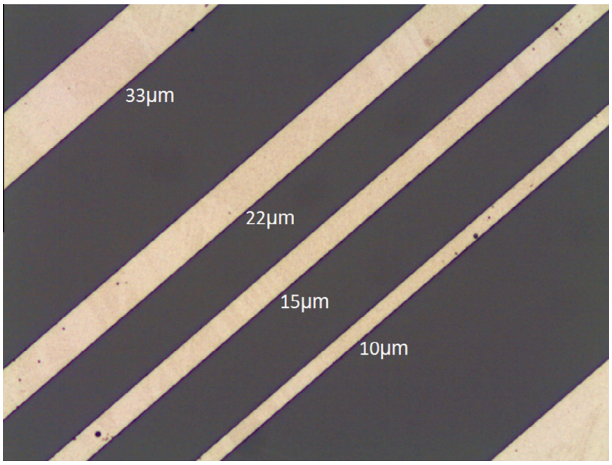

Fig. 3. Micrograph of Cr mask.

6.35 mm thick (12 × 12 mm) and Quartz wafer was used as a carrier wafer (2″). This set up led to insufficient cooling of the etched surface, which had two major effects on surface quality: formation of micro-crystallites and lack of surface homogeneity across the sample.

Fig. 4 shows micro-crystallites observed on bottom etched surface in some parts of the sample using an optical microscope and SEM after ICP etching. These crystallites evolved during etching and give further evidence for the high temperature of the sample during etching. No thermal sensors indicating the actual sample surface temperature were available; however the crystalline-phase was identified as α-cristobalite which is known to form above 1300 °C using micro-Raman spectroscopy.

The basis for cross-sample inhomogeneity might be the enhancement of bias electric field near the sharp edges of the square etched sample [17]. In the case of insufficient cooling, the more rapid and aggressive plasma etching near the sample perimeters might lead to an increased generation of heat which in turn further increases the rate of the etching reaction near the sample edges, resulting in etching inhomogeneity. A simple indication of the radial temperature and etch rate distribution during etching is a larger silica etching depth measured near the sample's perimeter than in the center (25 vs. 20 μm). Another important indication relates to the difference in top surface roughness across the wafer. Assuming that the temperature of the peripheral areas was higher than the central area during ICP etching, it is reasonable to assume that the mask etch rate was also higher near the perimeter. As a result, the mask was completely etched in the peripheral area exposing the silica to sporadic ion bombardment which resulted in surface damage. Fig. 5 shows ICP etching results at three different distances from the center of the sample. Radial dependence of the top surface quality can be observed as the central area of the etched sample is relatively smooth (Fig. 5a) and increasing "rain drop" like damage is noticed in peripheral areas (Fig. 5b and c).

In an effort to improve cooling efficiency and homogeneity, the sample was placed on various carrier wafers with better heat conduction than quartz wafers used above. Si, Al coated Si, Sapphire and AlN all had some minor positive effect on resulted homogeneity. Thermally conductive lubricant also increased cooling efficiency by sealing the insulating vacuum gap between the carrier wafer and the FS sample. In successful experiments, 4″ non-oxidized Si wafer was used as a carrier and Fombline oil was employed in order to attach the samples to it. In addition, etching process was paused every 10 min to allow for cooling under N_2 flow in the chamber. Finally, the most critical parameter was found

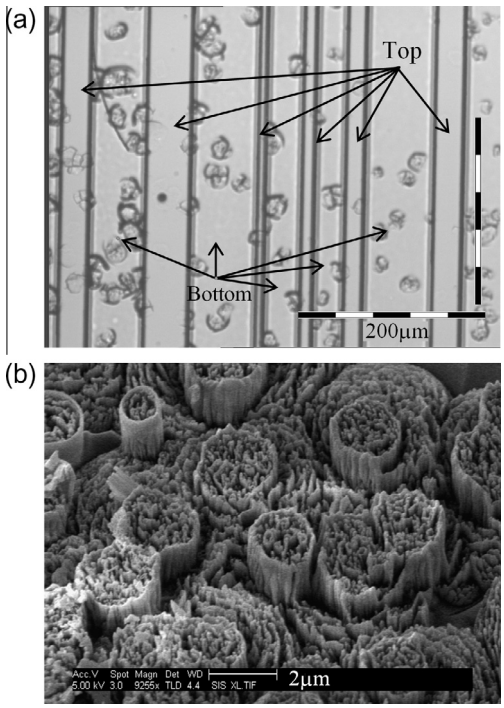

Fig. 4. Silica crystallites formed during ICP etching. (a) Optical microscope image. Notice crystallites formed mainly in areas that were not covered by Cr mask (etched surfaces) which were more significantly heated. (b) SEM image of crystalline area. Crystalline phase was identified as α-cristobalite using μ Raman measurements and indicate significant heating of the area during ICP etching to ~1300 °C.

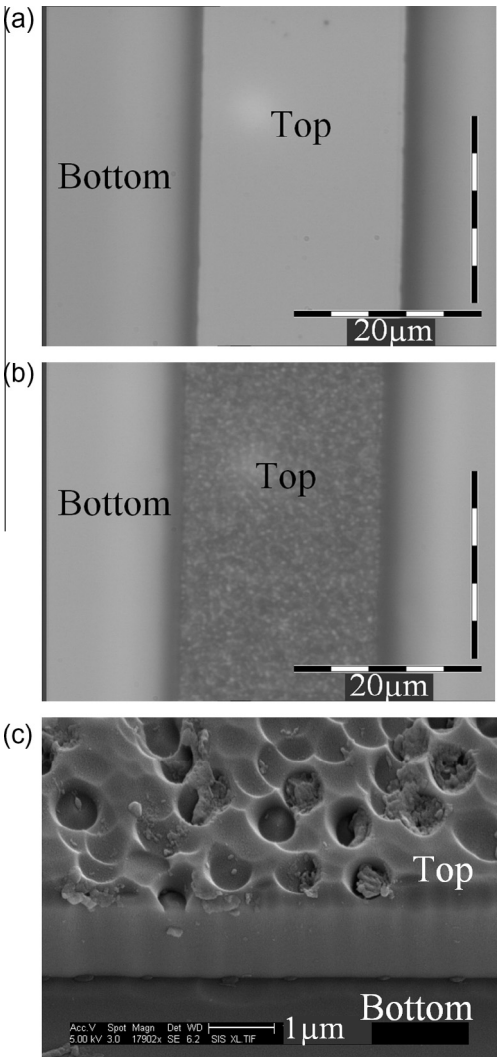

Fig. 5. Top-view micrographs of 22 μm wide silica waveguide etched using ICP process. (a) Central area of the sample where the Cr mask remained intact after etching, no surface damage is evident. (b) Peripheral area of the sample where the Cr mask was completely etched. (c) SEM image showing the poor surface quality of the top surface in the peripheral area of the sample where the mask was completely etched consequentially exposing the silica to sporadic ion bombardment.

to be the thickness of the pure silica substrate since FS is a poor heat conductor. Substrate was thinned from 6.35 mm to 300 μm which resulted in complete elimination of micro-crystallites and significantly improved homogeneity across the wafer. Substrate was not thinned further as this would make handling more difficult. Another result of thinning the sample was an increase in DC self-bias from −19 to −370 V and etch rate from 300 to 660 nm/min. Selectivity was also moderately improved from 1:7 to 1:8 as outlined in the line 1 of Table 1. Nevertheless, significant surface roughness was evident which was attributed to the etching chemistry as discussed below.

3.4. Gas mixture considerations in ICP etching of Yb/Al-codoped FS

Fluorine based chemistries, such as SF_6, CF_4 and C_4F_8 are commonly used to etch silica and are relatively selective to Cr mask. For example, a preliminary attempt to etch pure silica substrates using C_4F_8 (see 2nd line of Table 1 for process set parameters) showed good results with relatively high selectivity to Cr mask (1:35), etch rate of ~0.5 μm/min and overall homogeneity (see Fig. 6a). However, similar attempts to etch Yb/Al-codoped FS resulted in a high degree of roughness at the etched surface (see Fig. 6b).

One possible reason is a low etch rate of Al_2O_3, which is the phase of Al doping in silica, compared to silica using F chemistry etching. Al_2O_3 is often used as mask material for F chemistry based

Table 1
Summary of dry-etching process parameters and results. 1* refers to 6.35 mm thick samples whereas the rest refer to 0.3 mm.

#	Chemistry (sccm)	Pressure (mTorr)	ICP power (W)	Bias power (W)	DC self bias (V)	Etch rate (nm/min)	Selectivity	Results
1*	SF_6 (20), Ar (10)	3	1500	300	−19	300	1:7	Micro-crystallites
1.	SF_6 (20), Ar (10)	3	1500	300	−370	660	1:8	Rough surface
2.	C_4F_8 (27), O_2 (23)	5	2700	220	−100	300	1:9	Rough surface
3.	Cl_2 (30)	5	600	100	−30	0	0	Nearly no etching after 30 min
4.	Cl_2 (40), BCl_3 (10)	5	600	100	−50	26	1:1	Rough surface, no selectivity
5.	CF_4 (29), BCl_3 (5), Ar (10), O_2 (3.8)	5	800	300	−330	420	1:7	Smooth surface

etching processes [18] and so it is reasonable to assume that a large difference in etch rates exists. Energy-dispersive X-ray spectroscopy (EDX) was used to further study the result and showed F presence at the etched surface. One possible explanation for the observed roughness is that non-volatile AlF_3 was formed sporadically on the etched surface due to the Al doping [19,20]. AlF_3 is characterized by a low etch rate compared to fused silica [21] and may have induced roughness by randomly micro-masking the etched layer.

In attempt to avoid the effect, the gas mixture was changed and a heavy ion gas (Ar) was added to the Fluorine based plasma in order to promote physical etching of the Al component and/or removal of AlF_3 from the etched surface (see 1st line in Table 1). As a result, DC self-bias and etch rate grew significantly with a little change in selectivity. However, surface quality was only moderately improved with still unacceptable roughness amplitude in the order of 1 μm, and EDX measurements showed similar indications for micro-masking effect.

Based on these experiments, we had to conclude that Fluorine based chemistry, which is commonly used to etch pure silica, is unsuitable for Yb/Al-codoped FS.

Chlorine chemistries, such as Cl_2 and $SiCl_4$, are commonly used to etch Al_2O_3 [22] and are relatively selective to Cr mask. However, silica is known to be highly resistive to Chlorine based dry etching and often serve as a mask in such processes [23]. Preliminary experiments with Cl based chemistry (see lines 3–4 in Table 1) showed no etching process took place when the samples were exposed to Cl_2. Adding heavier BCl_3 ions induced effective physical etching of Al-doped FS. However, such physical etching caused by momentum exchange led to poor surface quality, even at relatively low DC bias of −50 V, and showed no selectivity to Cr mask.

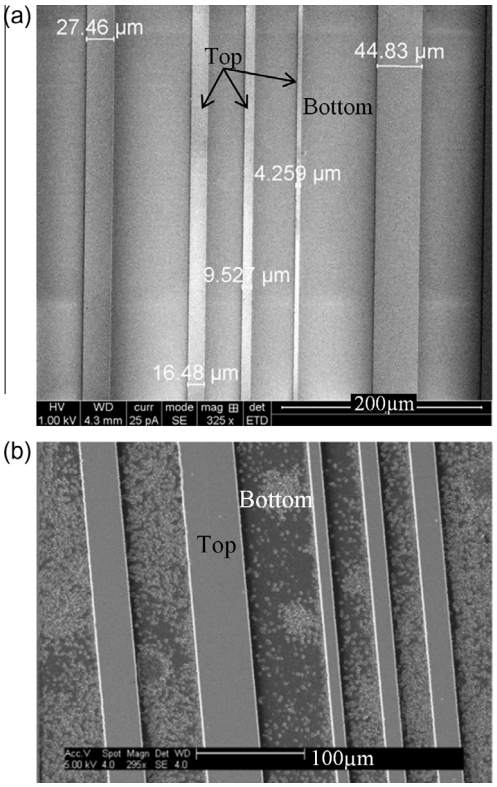

Fig. 6. (a) Pure FS after etching by C_4F_8. Note that the etched surface area has the same surface quality as the WG area which was protected by the mask. (b) Al/Yb-codoped FS after etching by C_4F_8. Note the poor surface quality in the etched surface probably caused by micro-masking of non-volatile AlF_3 created during the etching process.

Table 2
Role of etching chemistries.

Chemistry	Etch rate		Result
	Silica matrix	Al_2O_3 doping	
F	High	Low	Indication of micro-masking
Cl	Low	High	Nearly no etching occur

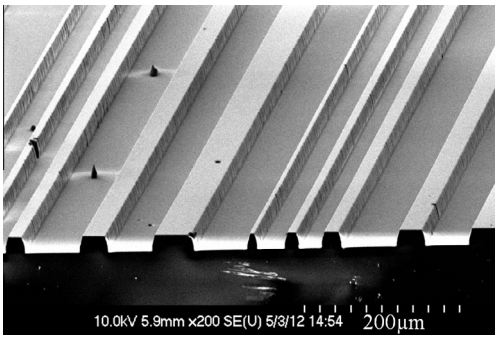

Fig. 7. SEM image of 20 μm depth etching of Yb/Al-codoped fused silica. WG widths vary from 10 to 50 μm. Etched surface is relatively smooth with sporadic defects.

Considering results summarized in Table 2, it is reasonable to suggest a combination of the two chemistries in a single etching process to successfully etch Yb/Al-codoped FS. Good results were achieved when alternating between CF_4 and BCl_3 (see 5th line in Table 1). O_2 was also used in order to increase etch rate of silica using CF_4 [24]. Fig. 7 shows 20 μm deep successful etching of Yb/Al-codoped FS with no signs of micro-masking effect, relatively smooth etched surface, 1:7 selectivity to Cr mask and good overall surface homogeneity. WGs are 1 cm long and 10–50 μm wide.

3.5. WG sidewall roughness

Fig. 7 shows the etched silica WGs are slightly trapezoidal in shape and significant WG sidewall roughness is evident in Fig. 8a.

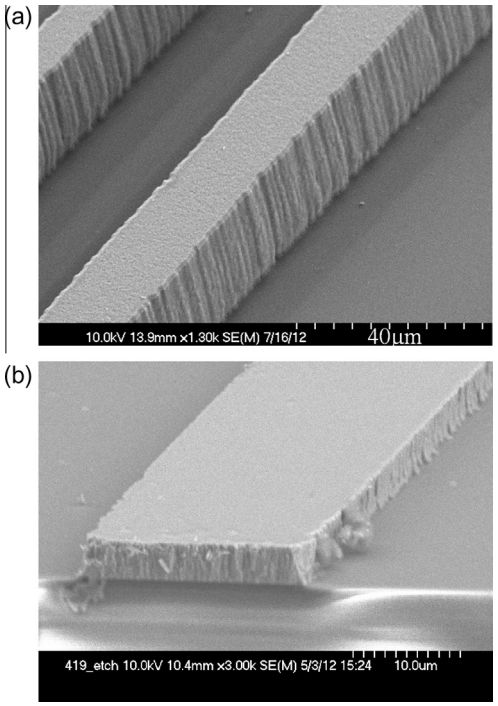

Fig. 8. (a) Detailed picture of 15 μm wide WG. Top Cr layer can be observed. Notice the WG sidewall roughness follows the remained mask LER. (b) Cr mask prior to ICP etching showing significant initial LER.

The shape of the WG affects the optical mode shape while the sidewall roughness leads to optical loss. Therefore it is important to understand the basis for both kinds of geometrical imperfections.

The origin for these phenomena is revealed by observing the SEM images of the Cr mask before and after ICP etching process. The remaining of the top Cr mask after ICP etching is visible in Fig. 8a and is 19.6 μm wide in contrast to 22 μm wide initial Cr stripe seen in Fig. 3. The mask recess during ICP etching might result in the trapezoidal shape of the silica WG. Regarding the WG sidewall roughness, Fig. 8a also shows that the WG sidewall roughness follows the LER of the remained Cr mask. Fig. 8b shows a 3 μm thick Cr mask stripe prior to ICP etching with significant LER characterized by similar amplitude and period as observed after etching. These findings indicate that a dominant part of the WG sidewall roughness is transferred from the mask to the etched WG sidewalls [25].

4. Optical characterization

The WGs facets were mechanically polished and a single mode laser beam (λ = 1030 nm, 20 mW) was end-coupled to the WG. The beam that propagates through the WG excites the Yb ions to fluoresce in all directions. Fig. 9 shows a fluorescence image captured by a top-view camera through a spectral filter ($\geqslant$1064 nm) which blocks the scattered light from the original input beam. As seen in the figure, the emission image is rather uniform without disruptions indicating a good structural quality of the WG. Note that reflections from the bottom-placed metallic sample-holder introduce some glare.

The WGs output facet plane was imaged with X25 magnification onto a CCD and shown in Fig. 10. The picture shows a nearly single mode structure, slightly asymmetrical due to the asymmetry of the WG (15 × 20 μm). The single mode operation was achieved by careful matching of the incoming beam spot to fit the lowest order mode of the WG. WG sidewall roughness may have contributed to maintain single mode operation since it preferably scatters high order modes into radiation [26].

Optical loss was measured by comparing the input and output powers, excluding the coupling loss by suitable spatial filtering. Preliminary results show typical values of optical loss in 1 cm long 33 × 20 μm WGs at 1030 nm are 1–2 dB/cm, depending on WG quality. Linear polarization state showed negligible effect on measured loss. Another method used to estimate the WGs optical loss is fluorescence streak imaging [27], where the decay in fluorescence power along the WG corresponds to the pump propagation loss, giving similar results. Note that the relatively small absorption at 1030 nm (~0.1 dB/cm) is negligible compared to the scattering loss. Interestingly, the loss figure measured for 2D rectangular WGs was roughly one order of magnitude higher than the loss measured for planar WGs prior to etching (0.2 dB/cm at 633 nm [16]. This shows that the rough silica-air interface at the WGs sidewalls induces significant light scattering and calls for further optimization of the process and cladding. In contrast, fluorescence lifetime and optical absorption values (0.8 ms, 5 dB/cm at 976 nm [15]) remained unchanged which shows that the etching process had no effect on Yb ions activity.

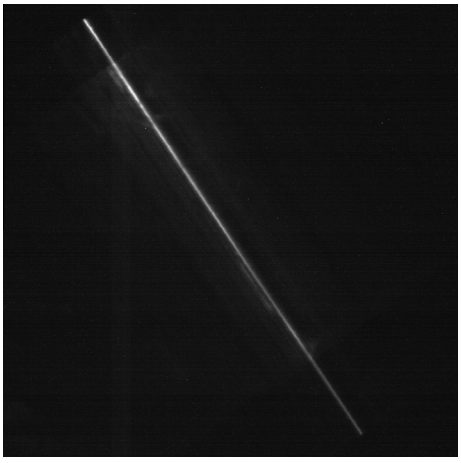

Fig. 9. Top view fluorescence image of 1 cm long Yb/Al-codoped silica waveguide. In-coupled light was 1030 nm while image was taken using a spectral filter $\lambda \geqslant$ 1064 nm.

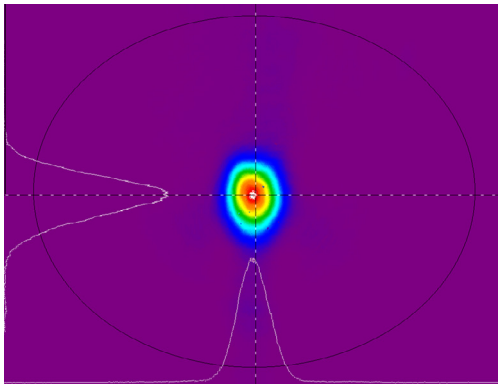

Fig. 10. WG facet output plane as captured by a CCD show nearly single-mode structure. Light scattering is evident around the mode area which is roughly 15 × 20 μm.

5. Conclusions

Fabrication method of 1D Yb/Al-codoped thick slab WGs (0.2 dB/cm optical loss), comprising direct nanoparticle deposition followed by amorphous sintering and laser heat treatment, was reported. In order to fabricate 2D rectangular WGs (~20 × 20 μm), the doped silica layers were subjected to Cr mask sputtering and photolithography followed by ICP etching. F and Cl based etching chemistries were individually investigated and a combined chemistry based alternately on BCl_3 and CF_4 was found suitable for deep ICP etching of Yb/Al-codoped silica. Cr mask (2.5 μm thick) was sputtered to meet the requirements of the relatively long chemical-physical etching process (1:7 selectivity, 0.4 μm/min). Silica crystallites observed on etched surface indicated significant heat is built up during etching (>1000 °C). Efficient cooling was found to be essential to avoid formation of crystallites and achieve cross-sample process homogeneity. Thermal management was successfully improved by thinning the FS substrate to 300 μm, replacing quartz wafer carrier with Si, and pausing the etching process every ten minutes to allow for sufficient cooling. Resultant sidewall roughness (evident in Fig. 8a) is relatively large, with ~0.5 μm amplitude as estimated from SEM images. Analyzing SEM images of the Cr mask before and after the etching process indicates that initial roughness of the Cr mask is transferred onto the silica WG sidewall and that the Cr mask is narrowed as a result of etching which may account for the trapezoidal shape of the silica WGs. LER is known as a major cause for loss in optical WGs and might be reduced by further optimizing lithography and etching process parameters. In addition, as described in Section 2, CO_2 laser heating was successfully used to smooth roughness in the doped silica layer prior to etching and might be further utilized to smooth WGs sidewall roughness. Future research is aimed to adjust the laser process parameters in order to "melt" and reduce sidewall

roughness in bulging rectangular FS WGs via surface-tension-driven melt-flow.

Finally, large core Yb/Al-codoped silica waveguides were successfully fabricated, with 10–50 μm width and 20 μm depth. Preliminary optical transmittance measurements show 1–2 dB/cm optical propagation loss for 33×20 μm WG at 1030 nm. We believe the results presented may constitute a significant progress towards on-chip high-power optical devices using silica-on-silica technology.

Acknowledgment

Helpful discussions and advice by Nurit Atar and Inbar Shani are greatly appreciated, as well as technical assistance by Avi Bloom.

References

[1] D. Richardson, J. Nilsson, W. Clarkson, J. Opt. Soc. Am. B: Opt. Phys. 27 (2010) B63–B92.
[2] J. Leger, J. Nillson, J. Huignard, A. Napartovich, T. Shay, A. Shirakawa, IEEE J. Sel. Top. Quantum Electron. 15 (2009) 237.
[3] C.J. Saraceno, O.H. Heckl, C.R.E. Baer, T. Südmeyer, U. Keller, Opt. Express 19 (2011) 1395–1407.
[4] R.A. Logan, F.K. Reinhart, J. Appl. Phys. 44 (2003) 4172–4176.
[5] B. Jalali, S. Yegnanarayanan, T. Yoon, T. Yoshimoto, I. Rendina, F. Coppinger, IEEE J. Sel. Top. Quantum Electron. 4 (1998) 938–947.
[6] A. Tervonen, B.R. West, S. Honkanen, Opt. Eng. 50 (2011) 071107.
[7] M. Kohtoku, T. Kominato, Y. Nasu, T. Shibata, NTT Tech. Rev. 3 (2005) 37–41.
[8] Y. Qiao, L. Wen, B. Wu, J. Ren, D. Chen, J. Qiu, Mater. Chem. Phys. 107 (2008) 488–491.
[9] G. Atar, D. Eger, O. Reinhardt, A. Bruner, B. Sfez, S. Ruschin, All-Fused-Silica Technology for On-Chip High Power Applications, Advanced Solid State Lasers, Optical Society of America, Paris, France, 2013. pp. AM4A. 31.
[10] M. Ams, G.D. Marshall, P. Dekker, M. Dubov, V.K. Mezentsev, I. Bennion, M.J. Withford, IEEE J. Sel. Top. Quantum Electron. 14 (2008) 1370–1381.
[11] A. Zoubir, M. Richardson, L. Canioni, A. Brocas, L. Sarger, J. Opt. Soc. Am. B 22 (2005) 2138–2143.
[12] J.F. Bauters, M.J. Heck, D.D. John, J.S. Barton, C.M. Bruinink, A. Leinse, R.G. Heideman, D.J. Blumenthal, J.E. Bowers, Opt. Express 19 (2011) 24090–24101.
[13] T. Chen, H. Lee, J. Li, O. Painter, K.J. Vahala, Ultra-Low-Loss Optical Delay Line on a Silicon Chip, Frontiers in Optics, Optical Society of America, 2011, p. FWS1.
[14] S. Tammela, M. Soderlund, J. Koponen, V. Philippov, P. Stenius, The potential of direct nanoparticle deposition for the next generation of optical fibers, in: Proceedings of SPIE Photonics West, Optical Components and Materials III 2006, p. 16.
[15] D. Eger, G. Atar, A. Bruner, B. Sfez, I. Juwiler, T. Kokki, P. Kykkaenen, Opt. Mater. 33 (2010) 438–443.
[16] G. Atar, D. Eger, A. Bruner, B. Sfez, M. Nathan, Opt. Mater. 34 (2012) 838–844.
[17] Y. Nishi, R. Doering, Handbook of Semiconductor Manufacturing Technology, CRC Press, 2000.
[18] H. Abe, M. Yoneda, N. Fujiwara, Jpn. J. Appl. Phys. 47 (2008) 1435.
[19] L. Lallement, C. Gosse, C. Cardinaud, M.-C. Peignon-Fernandez, A. Rhallabi, J. Vac. Sci. Technol., A 28 (2010) 277–286.
[20] E. Metwalli, C.G. Pantano, Nucl. Instrum. Methods Phys. Res., Sect. B 207 (2003) 21–27.
[21] D. Shin, J. Eo, J. Ceram. Process. Res. 6 (2005) 345.
[22] X. Yang, D.-P. Kim, D.-S. Um, D.-P. Kim, K.-T. Kim, J. Vacuum Sci. Technol. A: Vacuum, Surf., Films 27 (2009) 821–825.
[23] S. Zhou, B. Cao, S. Liu, Appl. Surf. Sci. 257 (2010) 905–910.
[24] S. Wolf, R.N. Tauber, Silicon Processing for the VLSI Era Vol. 1: Process Technology, Lattice Press, 1986.
[25] H. Namatsu, M. Nagase, T. Yamaguchi, K. Yamazaki, K. Kurihara, J. Vac. Sci. Technol., B 16 (1998) 3315–3321.
[26] P. Mazumder, S.L. Logunov, S. Raghavan, J. Appl. Phys. 96 (2004) 4042–4049.
[27] A. Kahn, Y. Kuzminykh, H. Scheife, G. Huber, JOSA B 24 (2007) 1571–1574.